bioRxiv preprint doi: https://doi.org/10.1101/2022.08.18.504053; this version posted August 19, 2022. The copyright holder for this preprint (which was not certified by peer review) is the author/funder, who has granted bioRxiv a license to display the preprint in perpetuity. It is made available under aCC-BY-NC-ND 4.0 International license.

Single-cell RNA sequencing highlights a reduced function of natural killer and cytotoxic T cell in recovered COVID-19 pregnant women

Nor Haslinda Abd Aziz[1#], Madhuri S. Salker[2#], Aditya Kumar Lankapalli[3], Mohammed Nasir Shafiee[1], Ersoy Kocak[5,6], Surya Sekhar Pal [2], Omer Khalid[2], Norhana Mohd Kasim[1], Aida Kalok[1], Norashikin Abdul Fuad[4], Stephan Ossowski[5,6], Nicolas Casadei[5,6], Deutsche COVID-19 OMICS Initiative (DeCOI), Sara Y Brucker[2], Olaf Riess[5,6], Yogesh Singh[2,5,6]*

[1]Department of Obstetrics and Gynaecology, Faculty of Medicine, Universiti Kebangsaan Malaysia Medical Centre, Kuala Lumpur, Malaysia
[2]Department of Women's Health, Research Institute for Women's Health, University of Tübingen, Tübingen, Germany
[3]Department of Life Sciences, University of Warwick, Coventry, UK
[4]Department of Obstetrics and Gynaecology, Sungai Buloh Hospital, Selangor, Malaysia
[5]Institute of Medical Genetics and Applied Genomics, University of Tübingen, Tübingen, Germany
[6]NGS Competence Centre Tübingen (NCCT), University of Tübingen, Tübingen, Germany

[#]Equal contributions

*Lead Contact for the study

Dr Yogesh Singh
Institute of Medical Genetics and Applied Genomics
NGS Competence Centre Tübingen (NCCT)
Research Institute of Women's Hospital
University of Tübingen
Calwerstraße 7, 72076, Tübingen
Germany
Email: yogesh.singh@med.uni-tuebingen.de

Key words: Pregnancy, COVID-19, PBMCs, NK cells and cytotoxic cells

Running title: Immune response in COVID-19 pregnant women

bioRxiv preprint doi: https://doi.org/10.1101/2022.08.18.504053; this version posted August 19, 2022. The copyright holder for this preprint (which was not certified by peer review) is the author/funder, who has granted bioRxiv a license to display the preprint in perpetuity. It is made available under aCC-BY-NC-ND 4.0 International license.

Abstract

Pregnancy is a complex phenomenon during which women undergo immense immunological change throughout this period. Having an infection with the SARS-CoV-2 virus leads to an additional burden on the highly stretched immune response. Some studies suggest that age-matched pregnant women are more prone to SARS-CoV-2 infection compared with normal healthy (non-pregnant) women, while alternative evidence proposed that pregnant women are neither susceptible nor develop severe symptoms. This discrepancy in different findings regarding the immune responses of pregnant women infected with SARS-CoV-2 virus is not well understood. In this study, we investigated how SARS-CoV-2 viral infection could modulate the immune landscape during the active infection phase and recovery in pregnant females. Using flow cytometry, we identified that intermediate effector $CD8^+$ T cells were increased in pregnant women who had recovered from COVID-19 as opposed to those currently infected. Similarly, an increase in $CD4^+$ T helper cells (early or late) during the recovered phase was observed during the recovery phase compared with infected pregnant women or healthy pregnant women, whilst infected pregnant women had a reduced number of late effector $CD4^+$ T cells. $CD3^+CD4^-CD8^-$NKT cells that diminished during active infection in contrast to healthy pregnant women were significant increase in recovered COVID-19 recovered pregnant women. Further, our single-cell RNA sequencing data revealed that infection of SARS-CoV-2 had changed the gene expression profile of monocytes, $CD4^+$ effector cells and antibody producing B cells in convalescent as opposed to healthy pregnant women. Additionally, several genes with cytotoxic function, interferon signalling type I & II, and pro- and anti-inflammatory functions in natural killer cells and $CD8^+$ cytotoxic T cells were compromised in recovered patients compared with healthy pregnant women. Overall, our study highlights that SARS-CoV-2 infection deranged the adaptive immune response in pregnant women and could be implicated in pregnancy complications in ongoing pregnancies.

bioRxiv preprint doi: https://doi.org/10.1101/2022.08.18.504053; this version posted August 19, 2022. The copyright holder for this preprint (which was not certified by peer review) is the author/funder, who has granted bioRxiv a license to display the preprint in perpetuity. It is made available under aCC-BY-NC-ND 4.0 International license.

Introduction

Corona virus disease-19 (COVID-19) is caused by SARS-CoV-2 virus which has led to a global pandemic since its emergence in Wuhan, China in late 2019 (Andersen *et al*, 2020; Zhou *et al*, 2020). More than 6.39 million people have died due to COVID-19 infection and more than 574.9 million people had been infected thus far (until 29.07.2022) (Medicine, 2022). However, these numbers are continuously rising due to newly emergent variants of this virus despite inoculation of COVID-19 vaccine worldwide (Kampf, 2021; Subramanian & Kumar, 2021).

Pregnancy is a complex phenomenon during which women undergo immense immunological changes throughout this period (Abu-Raya *et al*, 2020). During gestation several physiological changes in the anatomical structure of the respiratory system as well as in the immune system could pose a greater risk for the pregnancy complications in women (Bhatia & Chhabra, 2018). The immune system in pregnancy is always in a delicate balance; it must protect the semi-allogenic fetus from maternal rejection whilst simultaneously provide proper fetal development and protection against foreign pathogens (Aghaeepour *et al*, 2017; Watanabe *et al*, 1997). Epidemiological findings from other pandemics (e.g. influenza, Zika and Ebola) highlighted that pregnant women are more susceptible to severe complications and death from viral infection (Alberca *et al*, 2020; Silasi *et al*, 2015; Wilder-Smith, 2021). Having an infection with SARS-CoV-2 virus could hamper the over stretched immune response. Though, the real time number of infections in pregnant women appeared to be neglected due to limited studies (Nidhi, 2021). Global maternal and fetal outcomes have worsened during the COVID-19 pandemic such as increase in maternal death, pre-term labour, stillbirth, ruptured ectopic pregnancies and maternal depression (Henarejos-Castillo *et al*, 2020; Liu *et al*, 2020; Villar *et al*, 2021). Recent studies suggested that age matched pregnant women are more prone to SARS-CoV-2 infection compared with healthy non-pregnant women (Villar *et al.*, 2021). SARS-CoV-2 infection in pregnant mothers lead to increased placental inflammation, predisposition to the development of maternal vascular thrombosis, higher caesarean rate, fetal growth restriction and increased risk of preterm delivery (Wong *et al*, 2022). Additionally, altered villous maturation and severe-critical maternal COVID-19 infection were associated with an elevated risk of poor Apgar scores at birth and maternal mortality, respectively (Wong *et al.*, 2022). In contrast, other findings proposed that pregnant women are mostly asymptomatic (90%) and develop mild symptoms after SARS-CoV-2 infection (Mullins *et al*, 2020; Waghmare *et al*, 2021). However, the comparisons are based on small cohort and no global data is available on how the immune response of infected and recovered women is shaped by SARS-CoV-2 virus. A handful of studies investigated how the virus modules the function of immune cells during pregnancy (Bordt *et al*, 2021; Chen *et al*, 2021a; Chen *et al*, 2021b; Lu-Culligan *et al*, 2021; Ovies *et al*, 2021). Thus, there is no clear understanding why there is such a discrepancy in the immune response of pregnant women infected with SARS-CoV-2 virus in different published studies. In our study, we thus applied single-cell RNA sequencing (scRNA-seq) and

bioRxiv preprint doi: https://doi.org/10.1101/2022.08.18.504053; this version posted August 19, 2022. The copyright holder for this preprint (which was not certified by peer review) is the author/funder, who has granted bioRxiv a license to display the preprint in perpetuity. It is made available under aCC-BY-NC-ND 4.0 International license.

flowcytometry to investigate how SARS-CoV-2 viral infection could modulates the immune response during the active SARS-CoV-2 infection and after the recovery from COVID-19 disease in pregnant women.

Results

Demographics of the pregnant women:

A total of 19 pregnant Malaysian and Malaysian Indian pregnant women were enrolled for this study comprised of pregnant healthy controls (Preg-HC; n=11), pregnant SARS-CoV-2 infected (Preg-SARS-CoV-2; n=4), and the recovered from the SARS-CoV-2 infection (Preg-R; n=4), (Table 1) some of the same patients described in our recent published study (Cao *et al*, 2022). In Cao et al, 2022, we used plasma and PBMCs for intracellular cytokine staining and scRNA-seq and immunophenotyping is part of this study. Most of the infected pregnant women were either asymptomatic or some had mild/moderate manifestations of COVID-19. No severe form of COVID-19 was reported and used in this study. Most of the study participants were in third trimester including healthy control pregnant (except one participant which was in the second trimester), infected pregnant (except one participant which was in the second trimester) and recovered pregnant women (except one participant was in the second trimester) (Table 1).

Study ID	Age (years)	Ethnicity	1st PCR test	Symptoms*	WHO score**	Sample collection date*	Gestational age***
				Heathy control			
H1	33	Malay	-	Heathy control	-	24.11.20	36 weeks
H2	35	Malay	-	Heathy control	-	24.11.20	31 weeks
H3	29	Malay	-	Heathy control	-	24.11.20	38 weeks
H4	40	Malay	-	Heathy control	-	10.12.20	38 weeks
H5	34	Malay	-	Heathy control	-	14.12.20	38 weeks
H6	25	Indian	-	Heathy control	-	14.12.20	38 weeks
H7	31	Malay	-	Heathy control	-	14.12.20	35 weeks
H8	29	Malay	-	Heathy control	-	14.12.20	13 weeks
H9	37	Malay	-	Heathy control	-	15.12.20	37 weeks
H10	33	Malay	-	Heathy control	-	15.12.20	15 weeks
H11	27	Malay	-	Heathy control	-	16.12.20	38 weeks
H12	33	Malay	-	Heathy control	-	16.12.20	40 weeks
H13	31	Malay	-	Heathy control	-	16.12.20	25 weeks
				Infected			
D03	42	Malay	29.10.20	Asymptomatic_Inf	1	29.10.20	38 weeks
D07	26	Malay	27.08.20	Asymptomatic_Inf	1	27.08.20	23 weeks
D10	31	Indian	27.08.20	Asymptomatic_Inf	1	27.08.20	35 weeks
D14	29	Malay	14.10.20	Symptomatic$_Inf	2	14.10.20	38 weeks
				Recovered			
M02 ®	36	Malay	11.04.20	Symptomatic#_R	2	29.07.20	24 weeks
M05 (R)	36	Malay	11.04.20	Asymptomatic_R	1	13.04.20	36 weeks
M06 (R)	31	Malay	21.04.20	Asymptomatic_R	1	08.05.20	13 weeks
M20 ®	25	Malay	10.01.21	Symptomatic$_R	2	20.01.21	29 weeks
Notes:							

bioRxiv preprint doi: https://doi.org/10.1101/2022.08.18.504053; this version posted August 19, 2022. The copyright holder for this preprint (which was not certified by peer review) is the author/funder, who has granted bioRxiv a license to display the preprint in perpetuity. It is made available under aCC-BY-NC-ND 4.0 International license.

Symptoms* - Symptoms at the time of disease development.
WHO score** - WHO score at the disease development (1st PCR test).
Gestational age*** - Gestational age during the blood (PBMCs) sample collection.
Symptomatic$ - Fever for 2 days.
Symptomatic# - Cough for 2 days.
Symptomatic§ - Typical symptoms of COVID-19 disease such as fever, fatigue, cough, and loss of smell/taste etc.

Immunophenotyping of pregnant, pregnant infected and pregnant recovered women

In our cohort study most of the pregnant women were either infected or recovered and were asymptomatic or mild/moderately affected which is consistent with other previously reported findings (Waghmare *et al.*, 2021). We first explored the percentage of different immune subsets in peripheral blood mononuclear cells (PBMCs) to understand the distribution of immune cells in pregnant women. To understand this, we used 14-colour antibody panel to identify the different subtypes of T, B, NK cells and monocytes using flow cytometry. Gating strategy of live lymphocytes and monocytes is displayed in Supp. Fig.1. Overall, 200,000 cells were acquired for each sample and live cells were used for further analysis, we found significantly reduced lymphocytes (p=0.02 Preg-R vs Preg-HC; Kruskal-Wallis nonparametric test (p=0.01) and multiple comparisons based on post-hoc Dunn's test) in Preg-R patients compared with Preg-HC. Further, a reduced tendency in monocytes in Preg-SARS-CoV-2 and Preg-R patients compared with Preg-HC (Suppl. Fig. 1a, b). No obvious difference was observed either in $CD4^+$ or $CD8^+$ T cells among Preg-SARS-CoV-2, Preg-R patient samples, and Preg-HC, although, there was a tendency of decreased $CD8^+$ T cells and increased $CD4^+$ T cells in Preg-SARS-CoV-2 compared with Preg-R or Preg-HC, respectively (Suppl. Fig. 1c).

Early and late effector $CD4^+$ or $CD8^+$ T cells were dysregulated in Preg-SARS-CoV-2 and Preg-R

Further, all the samples were concatenated, and subjected to unsupervised clustering analysis using uniform manifold projection and approximation (UMAP) to classify the clustering of immune cells and identify the difference in immune cell subsets (Fig. 1a, b). We observed 5 major clusters of cells based on 14-colour flow parameters which includes monocytes, $CD4^+$ T cells, $CD8^+$ T cells, $CD19^+$ B cells and $CD56^+$ NK cells subsets. Further, using supervised clustering of $CD8^+$ T cells, we identified 5 different subsets of $CD8^+$ T cells (Fig. 1e). We found that naïve $CD8^+$ T cells were reduced in Preg-R patients compared with Preg-HC group and was almost significant (p=0.07) (Fig. 1f). Intermediate effector $CD8^+$ T cells were also significantly reduced in Preg-SARS-CoV-2 compared with Preg-R (p=0.03). Late effector $CD8^+$ T cells were also significantly reduced in Preg-SARS-CoV-2 compared with Preg-R (p=0.08), however, it did not reach to a significant level (Fig. 1f). This apparent effect was also observed in cell distribution UMAP analysis of $CD8^+$ T cells in Preg-SARS-CoV-2 compared with Preg-R (Fig. 1). Further, $CD4^+$ T cells were extracted and subject to unsupervised UMAP clustering analysis. We observed that

bioRxiv preprint doi: https://doi.org/10.1101/2022.08.18.504053; this version posted August 19, 2022. The copyright holder for this preprint (which was not certified by peer review) is the author/funder, who has granted bioRxiv a license to display the preprint in perpetuity. It is made available under aCC-BY-NC-ND 4.0 International license.

naïve T cells were reduced in Preg-SARS-CoV-2 and Preg-R compared with Preg-HC (Fig. 2a). Based on CD45RA and CCR7 markers, we found that early effector cells tended to increase in Preg-R compared with Preg-HC (p=0.07), though, it did not reach to significant level (Fig. 2b), however, late effector cells were increased in Preg-R compared with Preg-HC (Fig. 2b). Thus, it appears that naïve cells were reduced, whilst intermediate or later effector memory cells were increased in Preg-SARS-CoV-2 and Preg-R compared with HC.

Decreased $CD3^+CD4^-CD8^-$ NKT and NK cells in Preg-SARS-CoV-2 or Preg-R

Furthermore, the analysis of PBMCs showed reduced frequency of $CD3^+CD56^+$ NKT cells in Preg-SARS-CoV-2 infected women compared with Preg-HC (Fig. 2d, bottom, left). Interestingly, $CD3^+CD4^-CD8^-CD56^+$ NKT cells were significantly reduced in Preg-SARS-CoV-2 infected women compared with Preg-R (Fig. 2d, bottom, right). UMAP analysis depicted a clear distinction of NKT cells in Preg-SARS-CoV-2, Preg-R and Preg-HC. Further $CD3^-CD56^+$ NK cells were characterised using 2D FACS plots and unsupervised UMAP analysis. We observed that $CD3^-CD19^-CD56^+$HLA-DR^- NK cells were reduced in Preg-SARS-Co or Preg-R compared with HC (Fig. 3a, left). However, HLA-DR^+CD56^+ NK cells tended to be higher in Preg-SARS-CoV-2 or Preg-R compared with HC (Fig. 3a, right) and similarly, unsupervised clustering of $CD3^-CD19^-$ cells yielded a similar trend (Fig. 3b). Finally, we gated the $CD3^-CD19^-$ $CD56^+$HLA-DR^- NK and divided the NK cells in different subset using CD16 makers and found that mature $CD56^+CD16^+$ NK cells were decreased in Preg-SARS-CoV-2 or Preg-R compared with HC (Fig. 3c), the difference seen was not significant. Furthermore, non-NK cells were increased in Preg-SARS-CoV-2 and Preg-R (Fig. 3b, c). Overall, our data revealed that mature NK cell numbers were reduced, whilst increased number of activated NK cells in Preg-SARS-CoV-2 and Preg-R compared with Preg-HC.

Single cell gene expression profiling of Preg-R and Pre-HC

Flow cytometry results gave an insight at protein level, nonetheless, due to limitation of fluorochromes it is not possible to understand the expression of other molecules which might be affected in the Preg-R patients. We, therefore, employed single cell RNA-sequencing (scRNA-seq) gene expression profiling using the 10x chromium Gel Bead-in-Emulsion (GEMs) to verify this. We used 4 Preg-HC and 4 Preg-R samples for SC-RNA-seq. In total, we have obtained 45,859 high quality single cells for the cell clustering and gene expression analysis (Suppl. Fig. 2). Using ‘Seqgeq’ software, we first checked the library size versus genes expressed for high quality cells, secondly, we gated on high quality cells for total reads versus cells expressing genes and finally cells were gated for highly dispersed genes Suppl. Fig. 2b-c). Highly dispersed genes were used for PCA and PCA directed t-stochastic neighbour embedding (t-SNE) analysis – a statistical method visualizing high-dimension (Suppl. Fig. 2b-c). Further, using ‘Seurat’ plugin, we calculated the differential gene expression and cell clusters and explored different immune cell subsets (Suppl. Fig. 2d). We observed 20 cell clusters and have identified several major immune cells

bioRxiv preprint doi: https://doi.org/10.1101/2022.08.18.504053; this version posted August 19, 2022. The copyright holder for this preprint (which was not certified by peer review) is the author/funder, who has granted bioRxiv a license to display the preprint in perpetuity. It is made available under aCC-BY-NC-ND 4.0 International license.

populations – monocytes, dendritic cells, $CD4^+$ T cells, MAIT cells, $CD8^+$ T cells, NK cells, B cells and megakaryocytes (Suppl. Fig. 3d). Additionally, we overlaid the Preg-HC or Preg-R samples on all the samples with different cell clusters. There were a few instances where cell clusters were less abundantly present like naïve $CD4^+$ T cells, naïve B cells, NK cells and monocytes were reduced whereas MAIT cells were appeared to be present more in abundant in Preg-R samples compared with Preg-HC (Suppl. Fig. 2e). However, different subsets of $CD4^+$ or $CD8^+$ T cells were difficult to be distinguished.

Further, scRNA-seq analysis was performed using Seurat, performed the unsupervised clustering and visualized the data in Uniform Manifold Approximation and Projection (UMAP) plots. Cell clustering was based on PhonoGraph – a clustering algorithm, which is most robust when detecting refined subclusters (Liu *et al*, 2019). We discovered 34 cell subtypes of different immune cells (Fig. 4a). Further, individual known markers were defined to confirm the identity of a cell subtype group using unsupervised expression of each gene transcript (Fig. 4b-c). In detail, individual $CD4^+$ T cells were clustered into naïve, central memory (CM), effector memory (EM), cytotoxic $CD4^+$ T lymphocytes (CTL), SOX^+ $CD4^+$ T cells, and double negative (DN) cells. Similarly, $CD8^+$ T cells were also classified in naïve, EM, CM, CTL and MAIT cells and NK cells into 5 different type of NK cell population based on distinct cell clusters (Suppl. Fig. 3a-c). Moreover, individual expression of total cell clusters for Preg-R and Preg-HC showed a significantly decreased number of specific cell subsets $CD4^+$ CTL and B memory whilst $CD8^+$ CTLs were significantly increased in numbers (Fig. 4d-g). In contrary, NK II and NK IV were nearly significantly changed, and NK II tended to be increased whilst NK IV tented to be decreased in Preg-R compared with Preg-HC (Fig. 4f).

Differential pathway regulation in monocytes, B cells and $CD4^+$ TEM

Monocytes are the key innate immune cells in defence as well as ‘cytokine storm’ during COVID-19 pathology. We observed a clear reduced number of monocytes in Preg-R compared with Preg-HC. Thus, we explored the differential gene expression in Preg-R compared with Preg-HC, our data revealed that 329 genes were upregulated whilst 222 genes downregulated (Fold change ≥0.5 and q value ≤0.05) in Preg-R women (Fig. 5a). Based on upregulated genes, we performed Gene ontology pathway analysis using Metascape. We identified that Preg-R women had increased inflammatory gene signature which are mostly related with cytokine production, cell activation and regulation of defence response. Further, GO pathways suggested that TNF signalling pathways, catabolic process, lipid and orexin receptor pathways were also involved (Fig. 5b).

Further, B cells which are involved in humoral immune response were reduced in Preg-R and gene expression analysis highlighted that several genes were differentially regulated (349 upregulated and 229 downregulated) (Fig. 5c). The GO pathway analysis revealed that B cell receptor signalling pathways and extracellular

bioRxiv preprint doi: https://doi.org/10.1101/2022.08.18.504053; this version posted August 19, 2022. The copyright holder for this preprint (which was not certified by peer review) is the author/funder, who has granted bioRxiv a license to display the preprint in perpetuity. It is made available under aCC-BY-NC-ND 4.0 International license.

B cell activation by SARS-CoV-2 were upregulated (Fig. 5d). Furthermore, GO pathways were related with mRNA processing, chromatin organization and histone lysine methylation which could be involved in imprinting of IgG antibody formation.

$CD4^+$ TEM cells were also differentially abundant in Preg-R women, therefore, we also explored the differential (43 upregulated and 90 downregulated) gene expression and found that several genes were upregulated whilst 2-fold genes were downregulated (Fig. 5e). GO pathway analysis revealed that mRNA catabolic process was positively regulated, and further pathways related with regulation of inflammatory response, interferon type I signalling pathways, cell proliferation, apoptosis, cell division and epigenetic were upregulated (Fig. 5f).

NK, MAIT and $CD8^+$ T cell had reduced cytotoxic functions

Previously, we and others have shown that NK cell and $CD8^+$ T cells were decreased in moderate and recovered COVID-19 patients respectively (Maucourant *et al*, 2020; Singh *et al*, 2021; Tian *et al*, 2021) and both cell types decreased with increased severity of the disease. MAIT cells were also involved in COVID-19 infection (Chen *et al.*, 2021b). MAIT cells express the receptors for type I IFNs, IL-12, IL-15 and IL-18 thus these cells could potentially be activated by proinflammatory cytokines (Raffetseder *et al*, 2021). We therefore, explored the markers related with NK cells, MAIT and $CD8^+$ CTLs functions in pregnant women recovered after SARS-CoV-2 viral infection. GO pathway analysis for NK type II cells based on upregulated genes (13 genes only) revealed upregulation of chromatin organization and regulation of cell adhesion molecules, whist based several down regulated gene were related with perforin and granzymes (Fig. 6a, b). GO enrichment pathways (based on 82 downregulated genes) revealed that several pathways - cell activation, cytokine signalling, natural killer cell mediated cytotoxicity, and oxidative phosphorylation, SARS-CoV-2 signalling pathways were downregulated. These pathways have some common genes such as GZMB, IL32 and IRF9 which were downregulated in Preg-R women compared with Preg-HC (Fig. 6c, d). In a similar fashion in NK type IV cells, mRNA metabolic pathway, cytokine signalling, cellular response to stress and hypoxia were upregulated (based on 264 genes) whilst, antigen processing and presentation, natural killer cell mediated cytotoxicity, neutrophil degranulation, SARS-CoV-2 network signalling pathway, interferon alpha/beta signalling and cytokine signalling were downregulated (218 genes) in Preg-R compared with Preg-HC (Fig. 6e-g). The most common genes related with cytotoxic functions and cell activation including CD2, FCFR3A, KLRC2, TUBB, IL2RB, AREG, GNLY, GZMK and GZMA were significantly downregulated in Preg-R compared with Preg-HC (Fig. 6h).

MAIT cells which are involved in direct recognition of peptide without MHC molecules were also differentially expressed genes in Preg-R (250 genes up and 162 genes downregulated) compared with Preg-HC (Suppl. Fig. 4a). Several GO pathways were upregulated in Preg-R compared with Preg-HC which are related with mRNA

bioRxiv preprint doi: https://doi.org/10.1101/2022.08.18.504053; this version posted August 19, 2022. The copyright holder for this preprint (which was not certified by peer review) is the author/funder, who has granted bioRxiv a license to display the preprint in perpetuity. It is made available under aCC-BY-NC-ND 4.0 International license.

metabolic progress and cellular response to stress as well as cell adhesion. More interestingly, inflammatory, and anti-inflammation pathways such as IL-1, IFNs type I and TGB-b receptor signalling were also upregulated in Preg-R compared with Preg-HC (Suppl. Fig. 4b).

Moreover, in case of $CD8^+$ CTLs cells, several cytokines signalling pathway related were upregulated whilst, cytotoxic function pathway genes were downregulated. GO pathway analysis revealed that inflammation related pathways including TNF/NFkB, IFNG, VEGFA-VEGFR2, HIF and actin cytoskeleton pathways were upregulated (Fig. 6i-j), whilst adaptive immune system, type II interferon signalling, antigen processing and presentation of exogenous peptide antigen via MHC I, neutrophil degranulation and leukocyte mediated cytotoxicity were downregulated in Preg-R. The most common gene related with cytotoxic functions CD2, GZMK, HLA-A, KLRK1, KLDR1, GZMK, GZMA, GZMM, IL-32 and IL2RG were significantly downregulated in Preg-R compared with Preg-HC (Suppl. Fig. 4c-d).

Attenuated antiviral activity in recovered pregnant women

Previously, it was reported that after SARS-CoV-2 viral infection immunity is decreased in COVID-19 patients (Chua *et al*, 2020; Kim & Shin, 2021), thus, we investigated the status of their immune system. We discovered that expression of type I interferons (IFNs) receptors IFNAR1 and IFNAR2 was overall decreased in all immune cells, however IFNAR1 appeared to drastically decrease in B cell population (Fig. 7a). Downstream of type I IFNs signalling pathways TYK2, JAK1, STAT1, IRF9, ISG20, ISG20L2 and OAS3 were decrease in Preg-R patients (Fig. 7a). Type II IFNs signalling molecules such as IFN-g were increased in cytotoxic T cells. IFNGR1 and TNF were decreased in monocytes whereas cytotoxic $CD8^+$ T cells and NK cells IFGR1 and TNF were increased in Preg-R patients compared with Preg-HC (Fig. 7b). JAK2 was also increased in monocytes in Preg-R patients compared with Preg-HC (Fig. 7b). Finally, TGFBI is upregulated in both $CD8^+$ T and NK cells in Preg-R compared with Preg-HC (Fig. 7b). Overall, the data suggested a decrease of pro-inflammatory signalling mechanism and upregulation of anti-inflammatory molecules in Preg-R patients.

Discussion

An immune-mediated cytokine response is the key driver for the severity of COVID-19 and resulting in a ‘cytokine storm’. In this report, using multi-colour flow cytometry and SC-RNA-seq, we have identified the immune signature during SARS-CoV-2 infection and in COVID-19 recovered pregnant women.Our multi-colour immunophenotyping data suggest that there was significant reduction in percentage of total lymphocytes whilst there was trend of decreased monocytes in SARS-CoV-2 infected and recovered pregnant women compared with healthy pregnant women. Our findings are further supported by recent data which also suggested that in pregnant recovered women there is a reduced proportion of lymphoid cells

bioRxiv preprint doi: https://doi.org/10.1101/2022.08.18.504053; this version posted August 19, 2022. The copyright holder for this preprint (which was not certified by peer review) is the author/funder, who has granted bioRxiv a license to display the preprint in perpetuity. It is made available under aCC-BY-NC-ND 4.0 International license.

compared with healthy pregnant women (Chen *et al.*, 2021b). Further, characterization of $CD4^+$ T cells or $CD8^+$ T cells revealed an increased percentage of early or late effector $CD8^+$ T cells in pregnant SARS-CoV2 infected compared with pregnant recovered women. A similar trend was also observed for the $CD4^+$ T cells effector cells. However, a reduced trend of effector cells either $CD4^+$ or $CD8^+$ T cells were also observed when comparisons were made between healthy control pregnant with SARS-CoV-2 pregnant women. These results imply that viral infection leads to transient reduction of effector cells which are increased in proportion once the viral is cleared. Our data agree with published findings which implied that moderate COVID-19 patients had increased reappearance of effector T cells compared with severe COVID-19 patients (Odak *et al*, 2020).

NK cells tended to be decreased in SARS-CoV2 and recovered pregnant compared with healthy pregnant women. Earlier studies reported no significant change in NK cells and suggested increased trend of NK cells in pregnant COVID-19 women (Chen *et al.*, 2021a). Overall, our phenotyping data suggest decreased effector T cells and NK cells could stop an exacerbated immune response during the active infection of pregnant COVID-19 women. Cytokine and chemokines detection in the plasma of pregnant SARS-CoV-2 infected women revealed reduced levels of IL-12(p70) and increased RANTES levels (Chen *et al.*, 2021a). These findings suggest that suppressed cytokine and chemokines levels could be helpful to avoid adverse outcome and have unique anti-SARS-CoV-2 response during pregnancy.

Furthermore, scRNA-seq revealed increased levels of effector $CD4^+$ or $CD8^+$ T cells in recovered pregnant compared with healthy pregnant women. Differential gene expression analysis of $CD4^+$ TEM in recovered pregnant women suggested that several genes with interferon type I and inflammatory signalling pathways were changed. It appears that effector $CD4^+$ T cells from recovered pregnant women has a strong protective effective arm, which may lead to a competitive advantage to avoid overt inflammation to protect the ongoing pregnancy. Further, $CD4^+$ cytotoxic T cells were decreased whilst $CD8^+$ cytotoxic T cells were significantly increased. Differential gene expression analysis of $CD8^+$ CTL suggested that several pathways related with cytokine signalling (TNF, IFNG and IL-15), VEGFA-VEGFR2, actin cytoskeleton and HIF1 pathways were upregulated in recovered pregnant women. Furthermore, MAIT cells also have increased mRNA metabolic, IL-1, chromatin organization, interferon type I, TGFB, histone modification and immune system development were upregulated. pMonocytes also had increased inflammatory response, positive regulation of cytokine and cell activation and regulation of defence response. In a similar fashion, in B memory cells from recovered pregnant women also had increased chromatin organization, histone lysine methylation and activation of extrafollicular by SARS-CoV-2 and regulation of B cell proliferation were upregulated. Thus, scRNA-seq analysis suggested that a clear molecular advantage of infected recovered women to avoid the pregnancy complications. However, further large-scale studies are warranted to confirm these data and findings.

bioRxiv preprint doi: https://doi.org/10.1101/2022.08.18.504053; this version posted August 19, 2022. The copyright holder for this preprint (which was not certified by peer review) is the author/funder, who has granted bioRxiv a license to display the preprint in perpetuity. It is made available under aCC-BY-NC-ND 4.0 International license.

Limitation of the study

Our results may have provided key information for future research work into how pregnant women are affected by SARS-CoV-2 infection. However, there are still some limitations to this study. First, our cohort sample size was relatively small as few pregnant women agreed to donate the blood samples to the transcriptomics study. Additionally, we were not able to recruit pregnant women with severe symptoms. Also, pregnancy state has a dynamic and evolving immune changes at different trimester ages, which could also affect the immune response to COVID-19 as the pregnant patients who enrolled in our research study mostly developed symptoms in the second and third trimester rather than in the first trimester.

Figure legends

Sup. Fig.1 Characterization of PBMCs from pregnant infected and recovered from SARS-CoV-2 infection

a. Gating strategy for the 14-colour flow cytometry panel. Based on FSC and SSC we removed the cell debris and gated on live cells. FSC-A and FSC-W was used to remove the doublets and focussed on single cells. In the next step, we removed the cells using Violet Live/dead staining. Finally, we again we used FSC-A vs SSC-A to gate lymphocytes and monocytes based on size and granularity. Lymphocytes were discriminated in CD19 and CD3 based on cell surface markers and CD3 cells were discriminated into CD4 and CD8 cells using CD4 and CD8a antibodies.
b. FSC-A vs SSC-A show the monocytes and lymphocyte gated population (upper side FACS plots). The percentage of lymphocytes and monocytes shown by violin plots (lower side) for Preg-HC, Preg-SARS-CoV-2 and Preg-R samples.
c. FACS plots for CD4 versus CD8a staining gated on CD3+ T cells (upper side). The percentage of $CD4^+$ and $CD8a^+$ T cells in Preg-HC, Preg-SARS-CoV-2 and Preg-R samples.

Fig.1 Immunophenotyping of PBMCs in pregnant SARS-CoV-2 infected and recovered patients

a. Unsupervised clustering of immune cells based on 14-colour flow cytometry panel. Two major clusters for lymphocytes and monocytes population using UMAP dimensional reduction method.
b. Supervised clustering of PBMCs based on gating strategy identified 7 main subsets of cells as shown in a colour coded UMAP plot including monocytes, $CD3^+CD4^+$ T cells, $CD3^+CD8a^+$ T cells, $CD3^+CD56^+$NKT cells $CD3^-CD19^+$ B cells, $CD3^-CD56^+$NK cells and $FOXP3^+$ Tregs.
c. Overlay of UMAP to show the Preg-HC (Cyan), Preg-R (pink) and Preg-D (orange). All the combined cells were shown in the background (grey).
d. Comparisons of immune cells in recovered and infected pregnant women.

bioRxiv preprint doi: https://doi.org/10.1101/2022.08.18.504053; this version posted August 19, 2022. The copyright holder for this preprint (which was not certified by peer review) is the author/funder, who has granted bioRxiv a license to display the preprint in perpetuity. It is made available under aCC-BY-NC-ND 4.0 International license.

e. Dynamics of cytotoxic $CD4^+$ T cells. Identification of naïve, memory and effector memory $CD4^+$ T cells based on CD45RA and CCR7 markers. FACS plots show the $CD45RA^+CCR7^+$ naïve, $CD45RA^-CCR7^+$ CM cells, $CD45RA^{+high}CCR7^-$ late EM, $CD45RA^{+mid}CCR7^+$ intermediate EM, $CD45RA^-CCR7^-$ early EM cells (upper FACS plots). The percentage of naïve, intermediate, and late EM cells shown in violin plots (lower panels). P values show the significance among Preg-HC, Preg-SARS-CoV-2 and Preg-R groups and compared using Wilcoxon test. P value <0.05 considered significant.
f. UMAP analysis of total $CD4^+$ T cells. UMAP overlay show the Preg-HC (Cyan), Preg-R (pink) and Preg-D (orange).
g. UMAP analysis for different $CD4^+$ T helper cells based on supervised clustering.

Fig. 2 Dysregulated cytotoxic $CD8^+$ T cells and NKT cells in infected and recovered pregnant women

a. Dynamics of cytotoxic $CD8^+$ T cells. Identification of naïve, memory and effector memory cytotoxic $CD8^+$ T cells based on CD45RA and CCR7 markers. FACS plots show the $CD45RA^+CCR7^+$ naïve, $CD45RA^-CCR7^+$ CM cells, $CD45RA^{+high}CCR7^-$ late EM, $CD45RA^{+mid}CCR7^+$ intermediate EM, $CD45RA^-CCR7^-$ early EM cells (upper FACS plots). The percentage of naïve, intermediate, and late EM cells shown in violin plots (lower panels). P values show the significance among Preg-HC, Preg-SARS-CoV-2 and Preg-R groups and compared using Wilcoxon test. P value <0.05 considered significant.
b. UMAP analysis of total $CD8a^+$ T cells. UMAP overlay show the Preg-HC (Cyan), Preg-R (pink) and Preg-D (orange).
c. UMAP analysis for different cytotoxic T cells based on supervised clustering.
d. UMAP plots show the distribution of NKT cells in $CD4^+$ and $CD8a^+$ T cell compartments.
e. FACS plots represent the expression of CD56 on $CD3^+CD8^+$ T cells (Upper FACS panel). The percentage of NKT cells displayed by violin plots among Preg-HC, Preg-SARS-CoV-2 and Preg-R groups and compared using Wilcoxon test. P value <0.05 considered significant.
f. Overlay of UMAP to show the Preg-HC (Cyan), Preg-R (pink) and Preg-D (orange) for NKT cells. All the combined samples were shown in background (grey).

Fig. 3 Decreased NK cells in infected and recovered pregnant women

a. The percentage of $CD3^-CD19^-CD56^+$HLA-DR^- NK cells shown in FACS plots (upper panel) and violin plots (lower panel) in Preg-HC, Preg-SARS-CoV-2 infected and Preg-R samples.
b. UMAP analysis of $CD3^-CD19^-$ cells for different subsets of NK cells based on CD56 and CD16 expression for the terminal, mature, early NK and non-NK

bioRxiv preprint doi: https://doi.org/10.1101/2022.08.18.504053; this version posted August 19, 2022. The copyright holder for this preprint (which was not certified by peer review) is the author/funder, who has granted bioRxiv a license to display the preprint in perpetuity. It is made available under aCC-BY-NC-ND 4.0 International license.

cells, while grey coloured cells show the all the samples containing NK cells (upper panel). UMAP overlay for different comparative groups (lower panel).

c. The percentage of different subsets of NK cells based on CD56 and CD16 makers. Cells were gated on $CD3^{-}CD19^{-}CD56^{+}HLA\text{-}DR^{-}$ for data acquisition. Upper panels show the expression of CD56 and CD16 and lower panel show the violin plots of different NK subsets including mature, intermediate, and terminal NK cells.

Suppl. Fig. 2 Quality check and t-SNE analysis for single cell RNA-seq data from healthy control and recovered pregnant women

a. Total 56,586 cells were recovered after sequencing from 8 samples (Preg-HC and Preg-R). First RNA-sequenced cells were gated for genes expressed vs library size, we found 45,859 high quality cells. Next high QC cells were analysed for cells expressing based on total read cut off min cells 5 were chosen for further analysis. Cells expressing highly dispersed gene were gated and used for PCA and t-SNE analyses.
b. Highly dispersed genes were subjected to PCA analysis, and we ran 25 principle components (PC).
c. PC guided unsupervised clustering analysis was used calculating t-SNE map.
d. For identification of cell clusters from t-SNE plots, we identified 3 major clusters – monocytes, lymphocytes and B cells as shown in arbitrary clusters. Further each cluster based on RNA transcript levels and divided into major cell types – CD4+ T cells, CD8+ T cells, NK cells, NKT, ILC/MAIT, p and cMonocytes, dendritic cells and megakaryocytes.
e. Overlay of pregnant healthy control and recovered pregnant t-SNE clustering show difference in cell clustering.

Fig. 4 Dysregulated CD8, NK and B cells in recovered pregnant women

a. SC-RNA-seq data were analyzed using Seqgeq software. Seurat and PhenoGraph pipelines were run to get the different subtype of immune cells. 13 different immune cells were identified based on distinct gene expression.
b. Overlay of UMAP analysis of Preg-HC and Preg-R patients.
c. Key markers for the validation of different immune cell clusters
d. Percentage of major cell types in Preg-HC and Preg-R patients.

Suppl. Fig. 3 Representation of individual clusters based on phonograph-based cell clustering

a. $CD4^{+}$ T cell cluster. 7 major subtypes of $CD4^{+}$ T cells were identified.
b. $CD8^{+}$ T cell cluster. 5 subtypes of $CD8^{+}$ T cells were defined based on gene expression.
c. Five subtypes of NK cells in pregnant healthy and COVID-19 recovered patients.

Fig. 5. Inflammatory monocytes, activated memory B and $CD4^{+}$ TEM cells in Preg-R

bioRxiv preprint doi: https://doi.org/10.1101/2022.08.18.504053; this version posted August 19, 2022. The copyright holder for this preprint (which was not certified by peer review) is the author/funder, who has granted bioRxiv a license to display the preprint in perpetuity. It is made available under aCC-BY-NC-ND 4.0 International license.

a. Differential gene expression analysis in monocytes in Preg-R vs Preg-HC. Volcano plots showed the significantly upregulated and downregulated genes.
b. GO pathway analysis based on upregulated genes in monocytes
c. Gene expression analysis in B memory cells.
d. GO pathways anaylsis based on upregulated genes.
e. Differential gene expression analysis in IL-7R^{+} CD4^{+} TEM. Volcano plots represent significantly up and downregulation.
f. GO pathways analysis based on upregulated genes in CD4^{+} TEM cells.

Fig. 6 Reduced cytotoxic functions of NK and CD8^{+} CTLs in Preg-R

a. Differential gene expression analysis in Preg-R of NK II cells. Most significantly genes are shown on the man.
b. GO pathways based on upregulated genes in NK II.
c. GO pathways based on downregulated genes in NK II.
d. Dot plots represented significantly up and downregulated genes (selected genes) in NK II.
e. Differential gene expression analysis in Preg-R of NK IV cells. Most significantly genes are shown on the map.
f. GO pathways based on upregulated genes in NK IV.
g. GO pathways based on downregulated genes in NK IV.
h. Dot plots represented significantly up and downregulated genes (selected genes) in NK I.
i. Differential gene expression analysis in Preg-R of NK IV cells. Most significantly genes are shown on the man.
j. GO pathways based on upregulated genes in NK VI.

Suppl. Fig. 4 Deregulated MAIT and CD8^{+} CLTs response in Preg-R

a. Differential gene expression analysis in Preg-R of MAIT cells. Most significantly genes are shown on the volcano plot.
b. GO pathways based on upregulated genes in MAIT cells.
c. GO pathways based on downregulated genes in CD8^{+} CTLs cells.
Dot plots represented significantly up and downregulated genes (selected genes) in CD8^{+} CTLs (Red = upregulated, Blue = Downregulated (0.005)).

Fig. 7 Dysregulated Type I and type II IFN signalling in recovered pregnant women.

a. Type I IFN signalling genes (IFNAR1, IFAR2, TYK2, JAK1, STAT1, IRF-9, ISG20, ISG20L2, OAS3 and OASL) and their corresponding expression level.
b. Type I IFN signalling gens (IFNG, IFNGR1, JAK2, TNF and TGFBI).

Material and methods

bioRxiv preprint doi: https://doi.org/10.1101/2022.08.18.504053; this version posted August 19, 2022. The copyright holder for this preprint (which was not certified by peer review) is the author/funder, who has granted bioRxiv a license to display the preprint in perpetuity. It is made available under aCC-BY-NC-ND 4.0 International license.

584 ***Ethics statement for the study participants***
585
586 This study is part of the overall study of the transcriptomic and protein analysis of
587 pregnant women with a history of COVID-19 infection at the epicentre of the COVID-
588 19 pandemic in Malaysia approved by Research Ethics Committee, National
589 University of Malaysia (JEP-2021-465) and from the Medical Research Ethics
590 Committee (MREC) of Ministry of Health Malaysia (ID-58736). This was a cross-
591 sectional study carried out in Malaysia with a total of 21 pregnant women fulfilling the
592 inclusion and exclusion criteria were selected using convenient sampling. 4 pregnant
593 women infected with SARS-CoV-2 virus, 4 pregnant women who recovered from
594 COVID-19 and 13 pregnant women from healthy controls were provided written
595 informed consent to participate in this study. Disease severity for this study was
596 determined by symptoms. These women were recruited from the obstetrics and
597 gynaecology clinic, outpatient clinical wards from April 2020 until Feburary 2021. The
598 study procedures were carried out in accordance with Declaration of Helsinki.
599
600 ***Cohort size and sample collection***
601
602 We collected blood from total 8 SARS-CoV-2 infected and recovered pregnant
603 women (n=4/group) and 13 pregnant women enrolled in the Department of
604 Obstetrics and Gynaecology, Universiti Kebangsaan Malaysia Medical Centre, Kuala
605 Lumpur, Malaysia. Written informed consent from patients was obtained (Universiti
606 Kebangsan Malaysia). Eligibility criteria included age >18 years and positive RT-
607 PCR test for infected and negative RT-PCR test for healthy control and recovered
608 pregnant women. To protect the identity of the enrolled pregnant women,
609 pseudonymized samples were sent to Tübingen University for single cell RNA-
610 sequencing (scRNA-seq) processing and analysis. Blood was collected from
611 pregnant women infected with SARS-CoV-2 virus 1-3 days after their hospital
612 admittance or prior their caesarean section delivery. From pregnant women
613 recovered from COVID-19 who were admitted in wards before delivery and pregnant
614 women from healthy controls who attended the outpatient clinic, 3-5 ml blood was
615 collected in a 5 ml plain and a 10 ml Lithium heparin vaccutainer tubes. Serum
616 isolation via centrifugation will be conducted immediately after collection. Human
617 Peripheral Blood Mononuclear Cell (PBMCs) were isolated by the standard Ficoll
618 method (Singh *et al.*, 2021).
619
620 ***Preparation of PBMCs for single cell RNA sequencing (scRNA-seq) and***
621 ***antibody (surface and intracellular proteins) staining for flow cytometry***
622 Frozen PBMCs were thawed at 37 ^{0}C in a water bath for 2 minutes or until a small
623 ice crystal remains. In a biosafety hood (Level 2), thawed cells slowly transferred to a
624 50 ml conical tube using a wide-bore pipette tip and rinsed the cryovial with 1 ml
625 warm complete RPMI1640 medium (RPMI1640, 10% FBS, anti/anti) dropwise (1
626 drop per 5 seconds) to the 50 ml of tubes while gently shaking the tube. Further,
627 sequentially diluted cells in the 50 ml tube by incremental 1:1 volume addition of

bioRxiv preprint doi: https://doi.org/10.1101/2022.08.18.504053; this version posted August 19, 2022. The copyright holder for this preprint (which was not certified by peer review) is the author/funder, who has granted bioRxiv a license to display the preprint in perpetuity. It is made available under aCC-BY-NC-ND 4.0 International license.

complete RPMI1640 medium for a total of 5 times with 1 minute wait between each addition (total volume 32 ml). After completion of adding the medium, tube was centrifuged at 400xg for 5 minutes at room temperature. Supernatant was discarded after centrifuge leaving 1 ml of medium was left and mixed the cells using regular bore pipette or 10ml of Pasteur pipette tip. After mixing, 19ml of complete RPMI1640 was added and washed the cells at 400xg for 5 minutes at room temperature to remove any remaining DMSO from the cells. Again, supernatant was discarded, and cells were resuspended in 2 ml of medium and cells were counted. After counting the cells $1x10^6$ cells were used for each 14 colour FACS panel and $0.5x10^6$ cells were used for single-cell RNA sequencing (SC-RNA-Seq).

Flowcytometry data analysis staining and data analysis

For flow cytometry staining, $1x10^6$ cells were taken in 96 well plate and washed with DPBS (Ca^{2+}/Mg^{2+} free). First, the cells were stained with 5 ul of live and dead dye (1:400 dilution in PBS) and stained the cells for 15 minutes in dark at room temperature. After incubation, cells were washed once with PBS and added 50ul of PBS into each well. 12 colour antibodies cocktail was made for the surface recognizing markers (CD3, CD4, CD8, CD19, CD56, HLA-DR, CD38, CD154, CD45R, CCR7, CD14, CD16) as reported earlier (Singh *et al.*, 2021). For each reaction, we used 2.5ul antibody as well as 5.0ul of superbright staining buffer (to distinguish two different antibody in the superbright colour). Cells were incubated with antibody cocktail for 30-40 minutes. After incubation, cells were washed with PBS and fixed using fix/permb buffer for 45 minutes. After fixation, cells were permeabilized using 1x permeabilization buffer and added 2ul of Foxp3 intracellular antibody and incubated at room temperature for 30-40 minutes. After incubation, cells were washed with PBS and cell samples were acquired on BD Fortessa flow cytometry. Data were analysed using Flow jo for 2D FACS plots dimensional reduction methods.

Sample preparation of SC-RNA-seq

Thawed $0.5x10^6$ cells washed 3x at 400xg for 5 minutes at room temperature with 1x staining buffer (Biolegend) and kept on ice during the live dead staining using acridine orange and propidium dye to measure the cell viability before proceeding for 10x experiments. We followed the 10x chromium SC-RNA-seq protocol. In brief, after measuring the cell viability, cells were loaded on 10x Chromium Chip.

Single cells were prepared in the Chromium Single Cell Gene Expression Solution using the Chromium Single Cell 3' Gel Bead, Chip, and Library Kits v1 (10x Genomics) as per the manufacturer's protocol. In all, 20,000 total cells were loaded to each channel with an average expected recovery of 6000-9000 cells. The cells were then partitioned into Gel Beads in Emulsion in the Chromium instrument, where cell lysis and barcoded reverse transcription of mRNA occurred, followed by amplification, shearing, and 3' adapter and sample index attachment. Libraries were quantified by QubitTM 2.0 Fluorometer (ThermoFisher) and fragment size was

bioRxiv preprint doi: https://doi.org/10.1101/2022.08.18.504053; this version posted August 19, 2022. The copyright holder for this preprint (which was not certified by peer review) is the author/funder, who has granted bioRxiv a license to display the preprint in perpetuity. It is made available under aCC-BY-NC-ND 4.0 International license.

controlled using 2100 Bioanalyzer with High Sensitivity DNA kit (Agilent). Sequencing was performed in paired-end mode with a S1 and S2 flow cell (100 cycles) using NovaSeq 6000 sequencer (Illumina) at NCCT, IMGAG, Tübingen, Germany.

For the 10× Genomics sequencing data alignment and quantification, the sequencing data were processed using the CellRanger software (v3.0.1) with default parameters and the GRCh38 v3.0.0 human reference genome.

scRNA-seq analysis by Seqgeq software (BD Bioscience) using Seurat and associated plugin

First, cell ranger filtered feature matrix files (.HD5 format) were concatenated in "Seqgeq" online browser user friendly software (BD Bioscience and Flow Jo). We used n=4 Preg-HC and n=4 Preg-R (in duplicate) samples for analysis (total cells recovered from sequencing; n=55,588). Before concatenations each matrix file was normalized (counts per 10,000) and adjusted transformation to reflect normalized ranges. Concatenated file was normalized (counts per 10,000) and performed the quality check (QC) as described online (https://www.flowjo.com/learn/flowjo-university/seqgeq). In brief, we firstly identified the library size and gene expressed in total to decide the good quality cells in cell view platform. We identified 81% cells (n=45,859) were good quality (Suppl. Fig 2) and use for deciding the gene cut off for the upper and lower limit and gated as high parameters in cell view platform. High quality gated genes were selected for highly dispersed genes. These dispersed genes (n=1200) were used for software inbuilt dimensional reduction platforms - principal component analysis (PCA) guided t-distributed stochastic neighbour embedding (t-SNE) analysis to present the data into biaxial plots, while preserving variance contained in biological populations. Further, "Seurat plugin" analyses to perform the unsupervised cell clustering and UMAP analysis including the if any batch corrections. The Seurat output resulted in 20 cell clusters. Cell clusters were further defined on Seurat UMAP using another plugin "Phenograph" which results in 31 cell clusters. Each cell cluster was defined on differential gene expression analysis with respected to the all the cell clusters.

Psuedotime trajectory of B cells

Monocle plugin was used for pseudotime trajectory to understand the B cell development. B cells were concatenated from Seurat output pipeline and were fed into Monocle plugin seqgeq software as default setting.

Differential gene expression in Preg-HC vs Preg-R

Each cell clusters were compared for differential gene expression Preg-R vs Preg-HC to identify the upregulated and downregulated gene expression for gene enrichment analysis. Volcano plots were used for identifying differentially regulated genes to asecertain genes expressed abov a certain fold change and statistically significant p-value. By default, p-Values are adjusted using False Discovery Rate

bioRxiv preprint doi: https://doi.org/10.1101/2022.08.18.504053; this version posted August 19, 2022. The copyright holder for this preprint (which was not certified by peer review) is the author/funder, who has granted bioRxiv a license to display the preprint in perpetuity. It is made available under aCC-BY-NC-ND 4.0 International license.

(FDR) is calculated according to the Benjamini-Hochberg algorithm and considered significant (q value ≤0.05).

Gene ontology (GO) pathway enrichments using Metascape

Differentially upregulated or downregulated genes from each cell clusters were used for GO pathway enrichment anlysis using online Metascape tool (https://metascape.org). In brief, Metascape first automatically converts the input identifiers (Entrez Gene ID, RefSeq, Ensembl ID, UnProt ID or Symbol) into Human Entrez Gene ID. We first identified all statistically enriched terms (can be GO/KEGG terms, canonical pathways, hall mark gene sets, etc., based on the default choices under Express Analysis). Accumulative hypergeometric p-values and enrichment factors were calculated and used for filtering and the remaining significant terms were then hierarchically clustered into a tree based on Kappa-statistical similarities among their gene memberships (used in NCI DAVID site). Then 0.3 kappa score was applied as the threshold to cast the tree into term clusters. The terms within each cluster are exported in the Excel spreadsheet named “Enrichment Analysis” and presented in bar diagram for selected pathways.

Statistics analysis

Cytometry data was analyzed using FlowJo 10.8.1. Statistical analyses were performed in GraphPad Prism 9.3.0, unless otherwise stated. The statistical details of the experiments are provided in the respective figure legends. Data plotted in linear scale were expressed as Mean ± Standard Deviation (SD). Mann–Whitney U or Wilcoxon rank-sum tests with Dunn’s post-hoc (for multiple comparisons) were applied for unpaired comparisons, respectively.

Author’s contributions

NHAA: Conceiving the study, blood sample collection, metadata collection, performing the experiments, data analysis

MSS: Conceiving the study, performing initial part of scRNA-seq sample preparation, data analysis, figure preparation, writing the manuscript

AKL: Single cell data analysis, discussion, preparation of the figures

MNS: Conceiving the study, metadata collection, funding acquisition

NMK, AK, and NAF: Blood sample collection, PBMCs preparation, metadata collection

SPS, OK: PBMCs preparation for the flow staining and acquisition of the samples on flow cytometry

EK: scRNA-seq data processing and data analysis

SO, NC, SYB, OR: Funding acquisition, provided tools for sc-RNA-seq, data analysis and discussion of the scRNA-seq data

DeCOI: tools and data discussion

YS: Conceiving the study, provide support for the experiments, data analysis, funding acquisition, writing the manuscript and overall project management

bioRxiv preprint doi: https://doi.org/10.1101/2022.08.18.504053; this version posted August 19, 2022. The copyright holder for this preprint (which was not certified by peer review) is the author/funder, who has granted bioRxiv a license to display the preprint in perpetuity. It is made available under aCC-BY-NC-ND 4.0 International license.

Acknowledgements

We thank all the pregnant women who participated in this study. All the lab members who participated in fruitful discussion and technical assistance.

DeCOI consortium

DeCOI members are presented in https://decoi.eu/members-of-decoi/

Funding for the study

This project is supported by Ferring Pharmaceuticals to YS. MSS and MNS were also independently supported by Ferring Pharmaceuticals to provide materials and tools for this project. NGS sequencing methods were funded and performed with the support of the DFG-funded NGS Competence Center Tübingen (INST 37/1049-1) and Project-ID 286/2020B01 – 428994620. MSS is supported by the Margarete von Wrangell (MvW 31-7635.41/118/3) habilitation scholarship co-funded by the Ministry of Science, Research, and the Arts (MWK) of the state of Baden-Württemberg and by the European Social Funds.

Conflict of Interest

The authors declare that the research was conducted in the absence of any commercial or financial relationships that could be construed as a potential conflict of interest.

Data and code availability

- The raw data generated by SC-RNA-sequencing from this study are available to download through the public repository via the following accession number or link:
- This paper does not report any original code.
- Any additional information required to re-analyze the data reported in this paper is available from the lead contact upon reasonable request.

Lead contact

Requests for resources and reagents and for further information should be directed to and will be fulfilled by the Lead contact: yogesh.singh@med.uni-tuebingen.de

Literature:

Abu-Raya B, Michalski C, Sadarangani M, Lavoie PM (2020) Maternal Immunological Adaptation During Normal Pregnancy. Front Immunol 11: 575197

Aghaeepour N, Ganio EA, McIlwain D, Tsai AS, Tingle M, Van Gassen S, Gaudilliere DK, Baca Q, McNeil L, Okada R et al (2017) An immune clock of human pregnancy. Sci Immunol 2

bioRxiv preprint doi: https://doi.org/10.1101/2022.08.18.504053; this version posted August 19, 2022. The copyright holder for this preprint (which was not certified by peer review) is the author/funder, who has granted bioRxiv a license to display the preprint in perpetuity. It is made available under aCC-BY-NC-ND 4.0 International license.

Alberca RW, Pereira NZ, Oliveira L, Gozzi-Silva SC, Sato MN (2020) Pregnancy, Viral Infection, and COVID-19. Front Immunol 11: 1672

Andersen KG, Rambaut A, Lipkin WI, Holmes EC, Garry RF (2020) The proximal origin of SARS-CoV-2. Nature Medicine

Bhatia P, Chhabra S (2018) Physiological and anatomical changes of pregnancy: Implications for anaesthesia. Indian J Anaesth 62: 651-657

Bordt EA, Shook LL, Atyeo C, Pullen KM, De Guzman RM, Meinsohn MC, Chauvin M, Fischinger S, Yockey LJ, James K et al (2021) Maternal SARS-CoV-2 infection elicits sexually dimorphic placental immune responses. Sci Transl Med 13: eabi7428

Cao H, Abd Aziz NH, Xavier JR, Shafiee MN, Kalok A, Jee B, Salker MS, Singh Y (2022) Dysregulated Exosomes Result in Suppression of the Immune Response of Pregnant COVID-19 Convalescent Women. Frontiers in Molecular Biosciences 9

Chen G, Liao Q, Ai J, Yang B, Bai H, Chen J, Liu F, Cao Y, Liu H, Li K (2021a) Immune Response to COVID-19 During Pregnancy. Front Immunol 12: 675476

Chen G, Zhang Y, Zhang Y, Ai J, Yang B, Cui M, Liao Q, Chen H, Bai H, Shang D et al (2021b) Differential immune responses in pregnant patients recovered from COVID-19. Signal Transduct Target Ther 6: 289

Chua RL, Lukassen S, Trump S, Hennig BP, Wendisch D, Pott F, Debnath O, Thurmann L, Kurth F, Volker MT et al (2020) COVID-19 severity correlates with airway epithelium-immune cell interactions identified by single-cell analysis. Nat Biotechnol 38: 970-979

Henarejos-Castillo I, Sebastian-Leon P, Devesa-Peiro A, Pellicer A, Diaz-Gimeno P (2020) SARS-CoV-2 infection risk assessment in the endometrium: viral infection-related gene expression across the menstrual cycle. Fertil Steril 114: 223-232

Kampf G (2021) The epidemiological relevance of the COVID-19-vaccinated population is increasing. Lancet Reg Health Eur 11: 100272

Kim YM, Shin EC (2021) Type I and III interferon responses in SARS-CoV-2 infection. Exp Mol Med 53: 750-760

Liu P, Zheng J, Yang P, Wang X, Wei C, Zhang S, Feng S, Lan J, He B, Zhao D et al (2020) The immunologic status of newborns born to SARS-CoV-2-infected mothers in Wuhan, China. J Allergy Clin Immunol 146: 101-109 e101

Liu X, Song W, Wong BY, Zhang T, Yu S, Lin GN, Ding X (2019) A comparison framework and guideline of clustering methods for mass cytometry data. Genome Biol 20: 297

Lu-Culligan A, Chavan AR, Vijayakumar P, Irshaid L, Courchaine EM, Milano KM, Tang Z, Pope SD, Song E, Vogels CBF et al (2021) Maternal respiratory SARS-CoV-2 infection in pregnancy is associated with a robust inflammatory response at the maternal-fetal interface. Med (N Y) 2: 591-610 e510

Maucourant C, Filipovic I, Ponzetta A, Aleman S, Cornillet M, Hertwig L, Strunz B, Lentini A, Reinius B, Brownlie D et al (2020) Natural killer cell immunotypes related to COVID-19 disease severity. Sci Immunol 5

Medicine JHU (2022) Corona Virus Resource Center: https://coronavirus.jhu.edu/map.html.

Mullins E, Evans D, Viner RM, O'Brien P, Morris E (2020) Coronavirus in pregnancy and delivery: rapid review. Ultrasound Obstet Gynecol 55: 586-592

Nidhi S (2021) How doese COVID affect moher and Baby? Nature 591

Odak I, Barros-Martins J, Bosnjak B, Stahl K, David S, Wiesner O, Busch M, Hoeper MM, Pink I, Welte T et al (2020) Reappearance of effector T cells is associated with recovery from COVID-19. EBioMedicine 57: 102885

bioRxiv preprint doi: https://doi.org/10.1101/2022.08.18.504053; this version posted August 19, 2022. The copyright holder for this preprint (which was not certified by peer review) is the author/funder, who has granted bioRxiv a license to display the preprint in perpetuity. It is made available under aCC-BY-NC-ND 4.0 International license.

852 Ovies C, Semmes EC, Coyne CB (2021) Pregnancy influences immune responses
853 to SARS-CoV-2. Sci Transl Med 13: eabm2070
854 Raffetseder J, Lindau R, van der Veen S, Berg G, Larsson M, Ernerudh J (2021)
855 MAIT Cells Balance the Requirements for Immune Tolerance and Anti-Microbial
856 Defense During Pregnancy. Front Immunol 12: 718168
857 Silasi M, Cardenas I, Kwon JY, Racicot K, Aldo P, Mor G (2015) Viral infections
858 during pregnancy. Am J Reprod Immunol 73: 199-213
859 Singh Y, Trautwein C, Fendel R, Krickeberg N, Berezhnoy G, Bissinger R, Ossowski
860 S, Salker MS, Casadei N, Riess O et al (2021) SARS-CoV-2 infection paralyzes
861 cytotoxic and metabolic functions of the immune cells. Heliyon 7: e07147
862 Subramanian SV, Kumar A (2021) Increases in COVID-19 are unrelated to levels of
863 vaccination across 68 countries and 2947 counties in the United States. Eur J
864 Epidemiol 36: 1237-1240
865 Tian Y, Carpp LN, Miller HER, Zager M, Newell EW, Gottardo R (2021) Single-cell
866 immunology of SARS-CoV-2 infection. Nat Biotechnol
867 Villar J, Ariff S, Gunier RB, Thiruvengadam R, Rauch S, Kholin A, Roggero P,
868 Prefumo F, do Vale MS, Cardona-Perez JA et al (2021) Maternal and Neonatal
869 Morbidity and Mortality Among Pregnant Women With and Without COVID-19
870 Infection: The INTERCOVID Multinational Cohort Study. JAMA Pediatr 175: 817-826
871 Waghmare R, Gajbhiye R, Mahajan NN, Modi D, Mukherjee S, Mahale SD (2021)
872 Universal screening identifies asymptomatic carriers of SARS-CoV-2 among
873 pregnant women in India. Eur J Obstet Gynecol Reprod Biol 256: 503-505
874 Watanabe M, Iwatani Y, Kaneda T, Hidaka Y, Mitsuda N, Morimoto Y, Amino N
875 (1997) Changes in T, B, and NK lymphocyte subsets during and after normal
876 pregnancy. Am J Reprod Immunol 37: 368-377
877 Wilder-Smith A (2021) COVID-19 in comparison with other emerging viral diseases:
878 risk of geographic spread via travel. Trop Dis Travel Med Vaccines 7: 3
879 Wong YP, Tan GC, Omar SZ, Mustangin M, Singh Y, Salker MS, Abd Aziz NH,
880 Shafiee MN (2022) SARS-CoV-2 Infection in Pregnancy: Placental
881 Histomorphological Patterns, Disease Severity and Perinatal Outcomes. Int J
882 Environ Res Public Health 19
883 Zhou P, Yang XL, Wang XG, Hu B, Zhang L, Zhang W, Si HR, Zhu Y, Li B, Huang
884 CL et al (2020) A pneumonia outbreak associated with a new coronavirus of
885 probable bat origin. Nature 579: 270-273
886

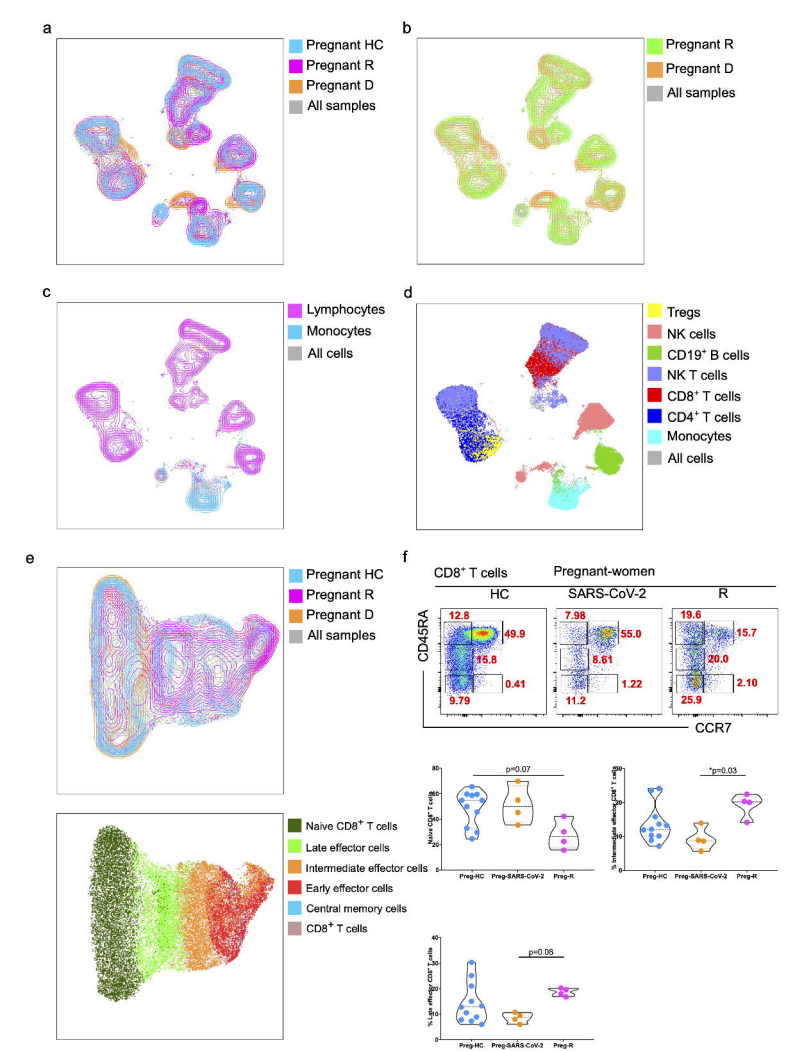
a
Pregnant HC
Pregnant R
Pregnant D
All samples
b
Pregnant R
Pregnant D
All samples
c
Lymphocytes
Monocytes
All cells
d
Tregs
NK cells
CD19+ B cells
NK T cells
CD8+ T cells
CD4+ T cells
Monocytes
All cells
e
Pregnant HC
Pregnant R
Pregnant D
All samples
Naive CD8+ T cells
Late effector cells
Intermediate effector cells
Early effector cells
Central memory cells
CD8+ T cells
f
CD8+ T cells
Pregnant-women
HC
SARS-CoV-2
R
CD45RA
CCR7
12.8
49.9
15.8
0.41
9.79
7.98
55.0
8.61
1.22
11.2
19.6
15.7
20.0
2.10
25.9
p=0.07
*p=0.03
p=0.06
Preg-HC
Preg-SARS-CoV-2
Preg-R

Fig. 1

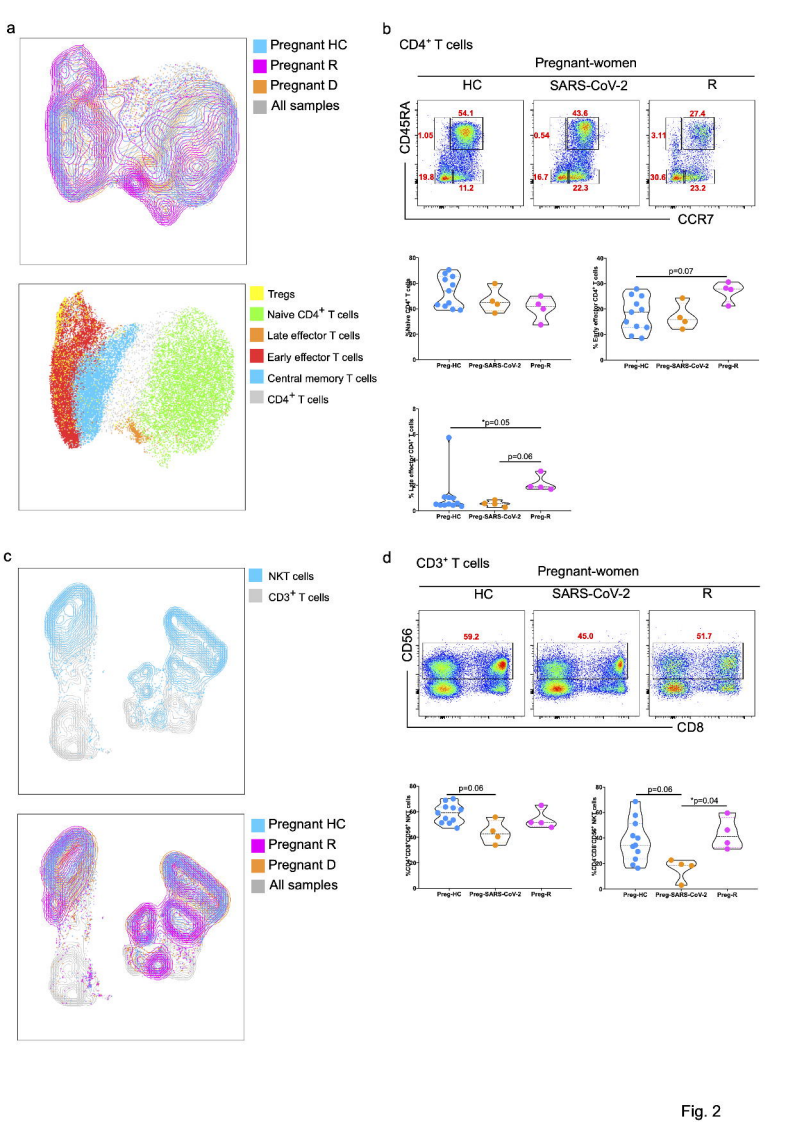
a
Pregnant HC
Pregnant R
Pregnant D
All samples
Tregs
Naive CD4+ T cells
Late effector T cells
Early effector T cells
Central memory T cells
CD4+ T cells
b
CD4+ T cells
Pregnant-women
HC
SARS-CoV-2
R
CD45RA
CCR7
54.1
1.05
19.8
11.2
43.6
0.54
16.7
22.3
27.4
3.11
30.6
23.2
p=0.07
Preg-HC
Preg-SARS-CoV-2
Preg-R
*p=0.05
p=0.06
c
NKT cells
CD3+ T cells
Pregnant HC
Pregnant R
Pregnant D
All samples
d
CD3+ T cells
Pregnant-women
HC
SARS-CoV-2
R
CD56
CD8
59.2
45.0
51.7
p=0.06
*p=0.04

Fig. 2

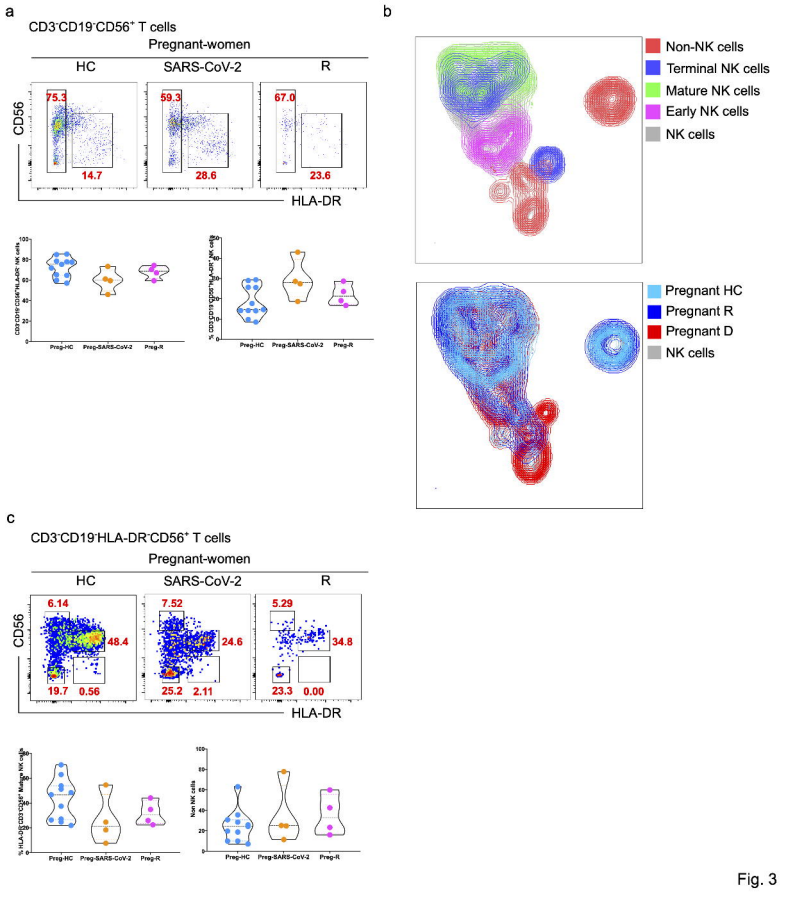
a
CD3-CD19-CD56+ T cells
Pregnant-women
HC
SARS-CoV-2
R
CD56
HLA-DR
75.3
14.7
59.3
28.6
67.0
23.6
Preg-HC
Preg-SARS-CoV-2
Preg-R
b
Non-NK cells
Terminal NK cells
Mature NK cells
Early NK cells
NK cells
Pregnant HC
Pregnant R
Pregnant D
NK cells
c
CD3-CD19-HLA-DR-CD56+ T cells
Pregnant-women
HC
SARS-CoV-2
R
CD56
HLA-DR
6.14
48.4
19.7
0.56
7.52
24.6
25.2
2.11
5.29
34.8
23.3
0.00
Preg-HC
Preg-SARS-CoV-2
Preg-R

Fig. 3

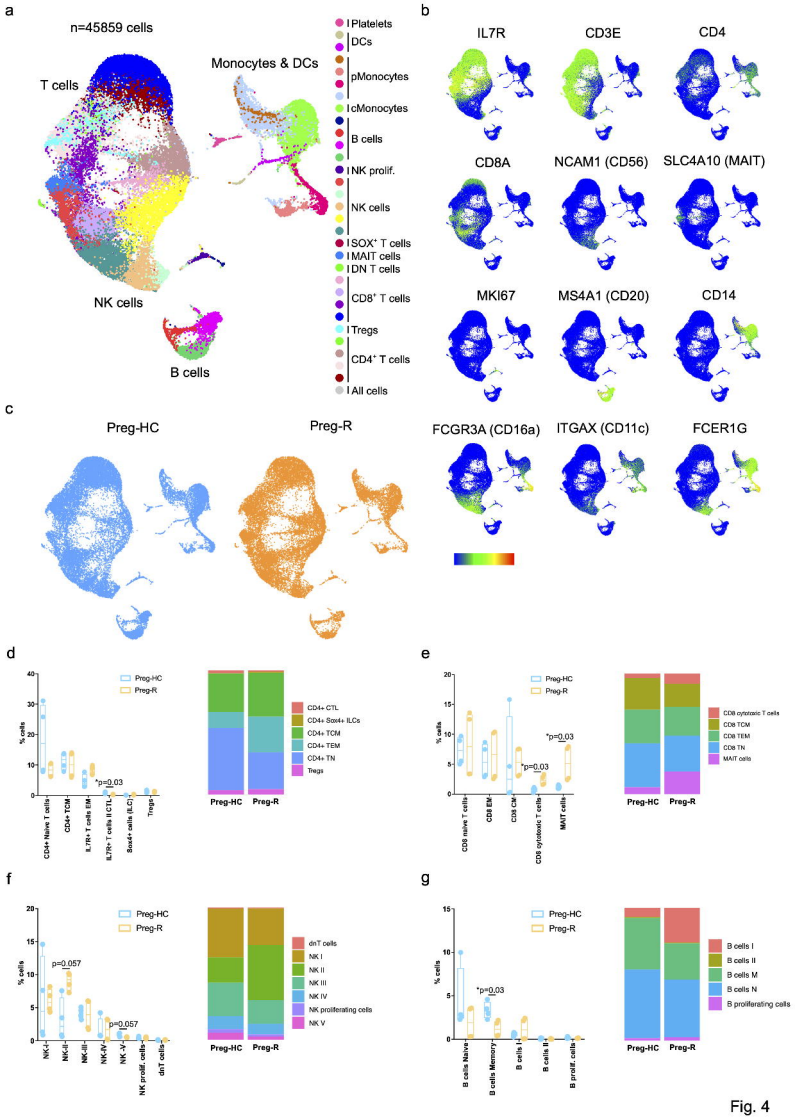
a
n=45859 cells
T cells
Monocytes & DCs
NK cells
B cells
Platelets
DCs
pMonocytes
cMonocytes
B cells
NK prolif.
NK cells
SOX+ T cells
MAIT cells
DN T cells
CD8+ T cells
Tregs
CD4+ T cells
All cells
b
IL7R
CD3E
CD4
CD8A
NCAM1 (CD56)
SLC4A10 (MAIT)
MKI67
MS4A1 (CD20)
CD14
c
Preg-HC
Preg-R
FCGR3A (CD16a)
ITGAX (CD11c)
FCER1G
d
Preg-HC
Preg-R
% cells
*p=0.03
CD4+ Naive T cells
CD4+ TCM
CD4+ TEM
IL7R+ T cells
IL17R+ T cells
Sox4+ cells (ILC)
Tregs
CD4+ CTL
CD4+ Sox4+ ILCs
CD4+ TCM
CD4+ TEM
CD4+ TN
Tregs
e
Preg-HC
Preg-R
% cells
*p=0.03
*p=0.03
CD8 naive T cells
CD8 EM
CD8 CM
CD8 cytotoxic T cells
MAIT cells
CD8 cytotoxic T cells
CD8 TCM
CD8 TEM
CD8 TN
MAIT cells
f
Preg-HC
Preg-R
% cells
p=0.057
p=0.057
NK-I
NK-II
NK-III
NK-IV
NK-V
NK prolif. cells
dnT cells
dnT cells
NK I
NK II
NK III
NK IV
NK proliferating cells
NK V
g
Preg-HC
Preg-R
% cells
*p=0.03
B cells Naive
B cells Memory
B cells I
B cells II
B prolif. cells
B cells I
B cells II
B cells M
B cells N
B proliferating cells

Fig. 4

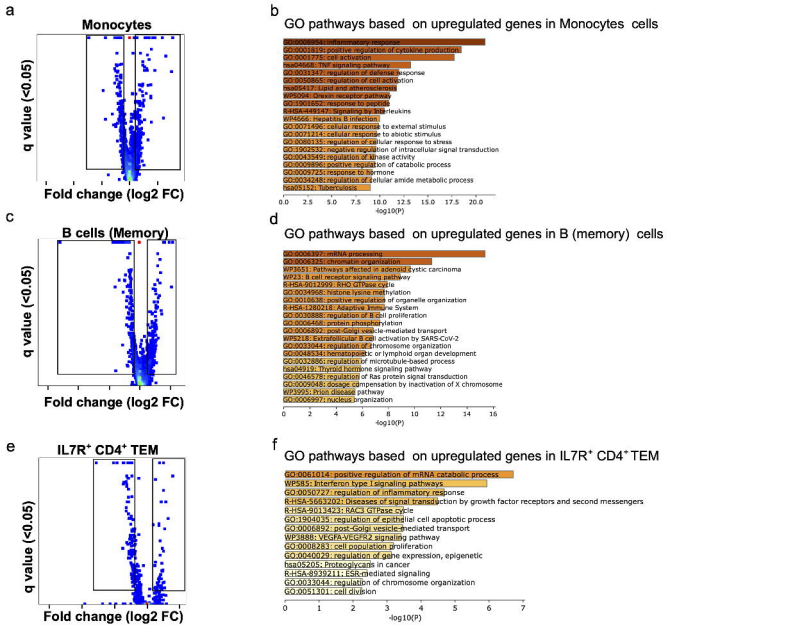
a
Monocytes
q value (<0.05)
Fold change (log2 FC)
b
GO pathways based on upregulated genes in Monocytes cells
GO:0002367: cytokine production involved
GO:0001819: positive regulation of cytokine production
GO:0001775: cell activation
hsa04668: TNF signaling pathway
GO:0031347: regulation of defense response
GO:0050863: regulation of cell activation
hsa05417: Lipid and atherosclerosis
WP5094: Oxavin receptor pathway
GO:1901652: response to peptide
R-HSA-449147: Signaling by Interleukins
WP4666: Hepatitis B infection
GO:0071496: cellular response to external stimulus
GO:0071214: cellular response to abiotic stimulus
GO:0080135: regulation of cellular response to stress
GO:1902532: negative regulation of intracellular signal transduction
GO:0043549: regulation of kinase activity
GO:0009896: positive regulation of catabolic process
GO:0009725: response to hormone
GO:0034248: regulation of cellular amide metabolic process
hsa05152: Tuberculosis
0.0 2.5 5.0 7.5 10.0 12.5 15.0 17.5 20.0
-log10(P)
c
B cells (Memory)
q value (<0.05)
Fold change (log2 FC)
d
GO pathways based on upregulated genes in B (memory) cells
GO:0006397: mRNA processing
GO:0006325: chromatin organization
WP3651: Pathways affected in adenoid cystic carcinoma
WP23: B cell receptor signaling pathway
R-HSA-8012999: RHO GTPase cycle
GO:0034968: histone lysine methylation
GO:0016638: positive regulation of organelle organization
R-HSA-1280218: Adaptive Immune System
GO:0030888: regulation of B cell proliferation
GO:0006468: protein phosphorylation
GO:0006892: post-Golgi vesicle-mediated transport
WP5218: Extrafollicular B cell activation by SARS-CoV-2
GO:0033044: regulation of chromosome organization
GO:0048534: hematopoietic or lymphoid organ development
GO:0031086: regulation of microtubule-based process
hsa04919: Thyroid hormone signaling pathway
GO:0046578: regulation of Ras protein signal transduction
GO:0009048: dosage compensation by inactivation of X chromosome
WP3995: Prion disease pathway
GO:0006997: nucleus organization
0 2 4 6 8 10 12 14 16
-log10(P)
e
IL7R+ CD4+ TEM
q value (<0.05)
Fold change (log2 FC)
f
GO pathways based on upregulated genes in IL7R+ CD4+ TEM
GO:0061014: positive regulation of mRNA catabolic process
WP585: Interferon type I signaling pathways
GO:0050727: regulation of inflammatory response
R-HSA-5663202: Diseases of signal transduction by growth factor receptors and second messengers
R-HSA-9013423: RAC3 GTPase cycle
GO:1904035: regulation of epithelial cell apoptotic process
GO:0006892: post-Golgi vesicle-mediated transport
WP3888: VEGFA-VEGFR2 signaling pathway
GO:0008283: cell population proliferation
GO:0040029: regulation of gene expression, epigenetic
hsa05205: Proteoglycans in cancer
R-HSA-8939211: ESR-mediated signaling
GO:0033044: regulation of chromosome organization
GO:0051301: cell division
0 1 2 3 4 5 6 7
-log10(P)

Fig. 5

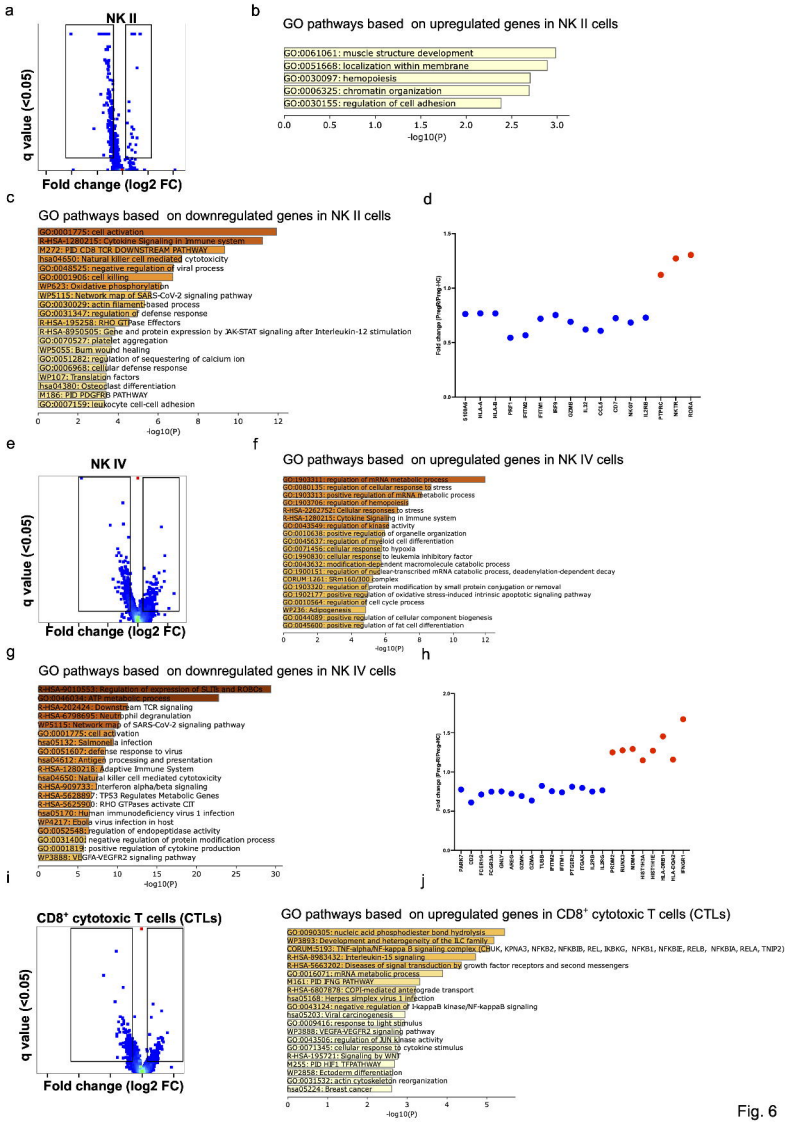
a
NK II
q value (<0.05)
Fold change (log2 FC)
b
GO pathways based on upregulated genes in NK II cells
GO:0061061: muscle structure development
GO:0051668: localization within membrane
GO:0030097: hemopoiesis
GO:0006325: chromatin organization
GO:0030155: regulation of cell adhesion
0.0 0.5 1.0 1.5 2.0 2.5 3.0
-log10(P)
c
GO pathways based on downregulated genes in NK II cells
GO:0001775: cell activation
R-HSA-1280215: Cytokine Signaling in Immune system
M2772: PID CD8 TCR DOWNSTREAM PATHWAY
hsa04650: Natural killer cell mediated cytotoxicity
GO:0048525: negative regulation of viral process
GO:0001906: cell killing
WP623: Oxidative phosphorylation
WP5115: Network map of SARS-CoV-2 signaling pathway
GO:0030029: actin filament-based process
GO:0031347: regulation of defense response
R-HSA-195258: RHO GTPase Effectors
R-HSA-8950505: Gene and protein expression by JAK-STAT signaling after Interleukin-12 stimulation
GO:0070527: platelet aggregation
WP5055: Burn wound healing
GO:0051282: regulation of sequestering of calcium ion
GO:0006968: cellular defense response
WP107: Translation factors
hsa04380: Osteoclast differentiation
M186: PID PDGFRB PATHWAY
GO:0007159: leukocyte cell-cell adhesion
0 2 4 6 8 10 12
-log10(P)
d
Fold change (Prog8/Prog16)
1.5
1.0
0.5
0.0
S100A8
HLA-A
HLA-B
PRF1
FITM2
FITM1
IER3
GZMH
IL32
CCL4
CD2
NKG7
IL2RB
PTPN6
NK-TR
HLA-I
e
NK IV
q value (<0.05)
Fold change (log2 FC)
f
GO pathways based on upregulated genes in NK IV cells
GO:1903311: regulation of mRNA metabolic process
GO:0080135: regulation of cellular response to stress
GO:1903313: positive regulation of mRNA metabolic process
GO:1903706: regulation of hemopoiesis
R-HSA-2262752: Cellular responses to stress
R-HSA-1280215: Cytokine Signaling in Immune system
GO:0043549: regulation of kinase activity
GO:0010638: positive regulation of organelle organization
GO:0045637: regulation of myeloid cell differentiation
GO:0071456: cellular response to hypoxia
GO:1990830: cellular response to leukemia inhibitory factor
GO:0043632: modification-dependent macromolecule catabolic process
GO:1900151: regulation of nuclear-transcribed mRNA catabolic process, deadenylation-dependent decay
CORUM 1261: SRm160/300 complex
GO:1903320: regulation of protein modification by small protein conjugation or removal
GO:1902177: positive regulation of oxidative stress-induced intrinsic apoptotic signaling pathway
GO:0010564: regulation of cell cycle process
WP236: Adipogenesis
GO:0044089: positive regulation of cellular component biogenesis
GO:0045600: positive regulation of fat cell differentiation
0 2 4 6 8 10 12
-log10(P)
g
GO pathways based on downregulated genes in NK IV cells
R-HSA-9010553: Regulation of expression of SLITs and ROBOs
GO:0016032: viral reproduction
R-HSA-202424: Downstream TCR signaling
R-HSA-6798695: Neutrophil degranulation
WP5115: Network map of SARS-CoV-2 signaling pathway
GO:0001775: cell activation
hsa05132: Salmonella infection
GO:0051607: defense response to virus
hsa04612: Antigen processing and presentation
R-HSA-1280218: Adaptive Immune System
hsa04650: Natural killer cell mediated cytotoxicity
R-HSA-909733: Interferon alpha/beta signaling
R-HSA-5628897: TP53 Regulates Metabolic Genes
R-HSA-5625900: RHO GTPases activate CIT
hsa05170: Human immunodeficiency virus 1 infection
WP4217: Ebola virus infection in host
GO:0052548: regulation of endopeptidase activity
GO:0031400: negative regulation of protein modification process
GO:0001819: positive regulation of cytokine production
WP3888: VEGFA-VEGFR2 signaling pathway
0 5 10 15 20 25 30
-log10(P)
h
Fold change (Prog8/Prog16)
2.0
1.5
1.0
0.5
0.0
RARA2
CD2
FCER1G
SCARA3
GNLY
AREG
GZMK
CCR7
TCEB3
IFITM2
FITM1
PTGDS
ITGA2
IL2RB
CD3D
PTGR1
RUNX3
KIRA4
HLA-DPA1
HIST1H1E
HLA-DRB1
HLA-DQA1
PPGR1
i
CD8⁺ cytotoxic T cells (CTLs)
q value (<0.05)
Fold change (log2 FC)
j
GO pathways based on upregulated genes in CD8⁺ cytotoxic T cells (CTLs)
GO:0090305: nucleic acid phosphodiester bond hydrolysis
WP3803: Development and heterogeneity of the ILC family
CORUM:5101: TNF-alpha/NF-kappa B signaling complex (CHUK, KPNA3, NFKB2, NFKBIB, REL, IKBKG, NFKB1, NFKBIE, RELB, NFKBIA, RELA, TNIP2)
R-HSA-8983432: Interleukin-15 signaling
R-HSA-5663202: Diseases of signal transduction by growth factor receptors and second messengers
GO:0016071: mRNA metabolic process
M161: PID IFNG PATHWAY
R-HSA-6807878: COPI-mediated anterograde transport
hsa05168: Herpes simplex virus 1 infection
GO:0043124: negative regulation of I-kappaB kinase/NF-kappaB signaling
hsa05203: Viral carcinogenesis
GO:0009416: response to light stimulus
WP3888: VEGFA-VEGFR2 signaling pathway
GO:0043506: regulation of JUN kinase activity
GO:0071345: cellular response to cytokine stimulus
R-HSA-195721: Signaling by WNT
M255: PID HIF1 TFPATHWAY
WP2858: Ectoderm differentiation
GO:0031532: actin cytoskeleton reorganization
hsa05224: Breast cancer
0 1 2 3 4 5
-log10(P)

Fig. 6

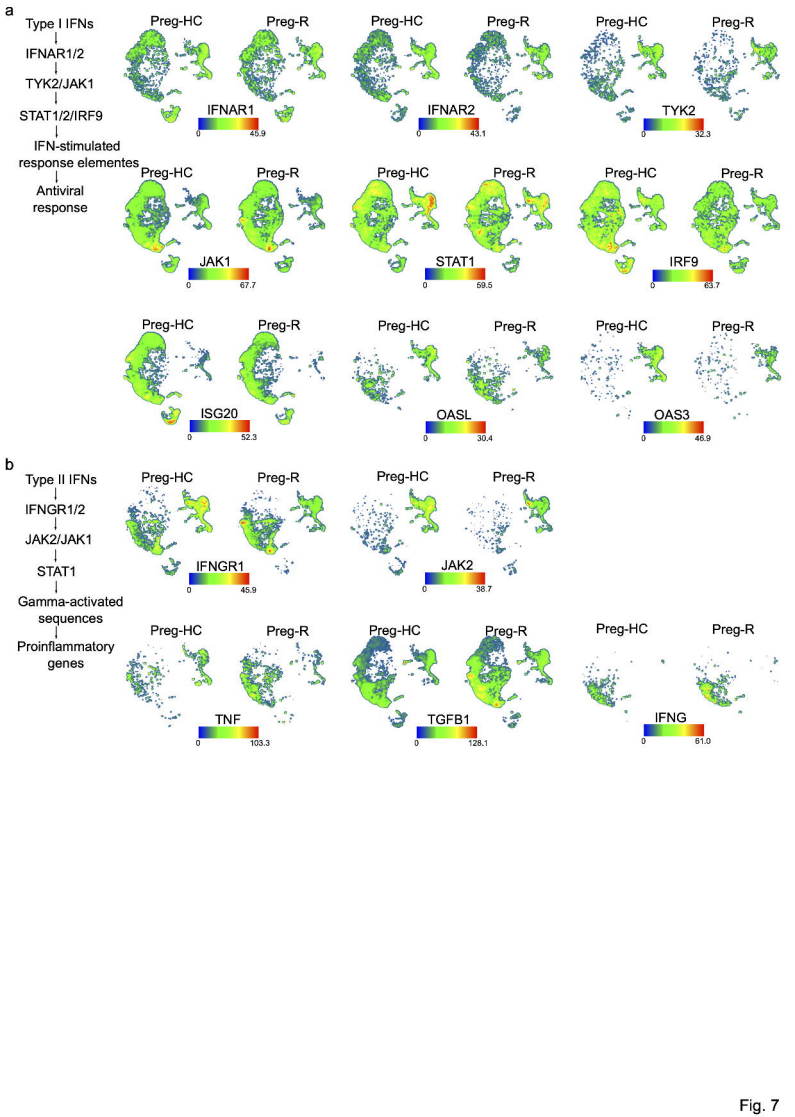
a
Type I IFNs
IFNAR1/2
TYK2/JAK1
STAT1/2/IRF9
IFN-stimulated response elementes
Antiviral response
Preg-HC
Preg-R
IFNAR1
0
45.9
IFNAR2
0
43.1
TYK2
0
32.3
JAK1
0
67.7
STAT1
0
59.5
IRF9
0
63.7
ISG20
0
52.3
OASL
0
30.4
OAS3
0
46.9
b
Type II IFNs
IFNGR1/2
JAK2/JAK1
STAT1
Gamma-activated sequences
Proinflammatory genes
IFNGR1
0
45.9
JAK2
0
38.7
TNF
0
103.3
TGFB1
0
128.1
IFNG
0
61.0

Fig. 7